

Preparation of Medical Composites for X-ray Shielding

Study of Filler Dispersion and Distribution



LIDIA SOLAZ BELANDO

Department of Materials and Manufacturing Technology
Chalmers University of Technology
Göteborg, Sweden 2015

Diploma work No. 165/2015

Performed at Department of Materials and Manufacturing Technology,
Chalmers University of Technology, Gothenburg, Sweden

Examiner: Prof. Antal Boldizar
Department of Materials and Manufacturing Technology
Chalmers University of Technology

Supervisors: Zebastian Bohström, PhD (Ten Medical Design AB)

1. Introduction

Projection radiography is an important medicinal diagnostic tool. The surgeon use radiation imaging in order to minimize invasive operations. The dentist use radiation imaging to perform intraoral and dental examinations. When using radiation imaging medicinal personal is exposed to radiation. To protect medicinal personal from radiation, protective garments are used. These protective garments incorporate lead or other high atomic number elements [1]. Such types of protective garments are generally considered heavy and expose the wearer to ergonomic risks, which often for the long time user, such as the surgeon leads to back strain and orthopedic problem [1]. Another problem with specifically lead, which provides high radiation protection is that it is classified as hazardous waste and therefore impose environmental and is subdued stringent disposal legalization [1]. There is a current market need for radiation protective garments that reduce the ergonomic risk of the wearer and that is composed of less hazardous high atom elements.

In this work we have used a model substance as filler material, CuO (low hazard filler) and an ethylene vinyl acetate (EVA) polymer to prepare a metal composite with X-ray protection properties. A composites X-ray protection properties is proportional to its composition as well as its filler dispersion and distribution [2]. The composite also need high filler content in order to provide satisfactory X-ray protection. High filler loading may impose mechanical problems restricting or hindering end processing of the material. Therefore the mechanical properties of composite filaments were evaluated with tensile strength tests according to a modified ISO rubber standard.

The focus of this thesis has been related to analysis of dispersion and distribution of CuO with two different particle sizes and particle size distributions i.e., Sigma-Aldrich (mean 0.9 μm and range 0-2.2 μm) and Fluka (mean 3.3 μm and range 1.0-31.0 μm). The final goal of the project has been to optimize extrusion and melt mixing conditions as to minimize particle aggregation, to maximize X-ray shielding properties of the composite material. X-ray radiation is a complicated natural scientific phenomenon and will not be further discussed in this thesis. For determination of filler particle size and particle size distribution scanning electron microscopy (SEM) was used. For evaluation of dispersion and distribution of low filler loaded composites (0.2 and 1.0 vol.%) light microscope was used. From the light microscope data a dispersion index was calculated according to the method outlined by T. Glaskova *et. al.* [3]. Capillary rheometer was used to determine K and n values in the power law for the viscosity η of non-newtonian liquids ($\eta=K\dot{\gamma}^{n-1}$). The empirical K and n values have been shown to be related to the presence of particle aggregates [4, 5].

The Master thesis has been carried out at the Materials and Manufacturing Technology Department at Chalmers University of Technology (CTH). The work has been executed in close cooperation with 10MD and Swerea IVF. All composite syntheses has been conducted at CTH and been carried out as a part of the thesis work. Extrusion was initiated at CTH but finally carried out at Swerea IVF. X-ray imaging and tensile strength testing has been done at Swerea IVF. All other analysis work has been carried out at CTH as a part of the thesis work.

2. Theory

2.1 Composites

Composites (composition materials) are multiphase materials made from two or more constituents with different chemical or physical properties. One material acts as a matrix (also called binder) and binds the filler. The filler consists of particles, fibers, laminates or gas [2]. Composites are usually classified according to type of filler material used: particle composites (flakes, beads, needles, spheres and irregular shaped); fiber composites (short and long also include laminates); gas-reinforced composites (foams), see Figure 1 [6, 7]. Particle composites are layered isotropically. Fiber composites can have both, isotropic and an anisotropic layered structure, while laminar composites always have anisotropic layers. The filler spatial configuration as well as shape and form affect mechanical properties such as tensile strength, stiffness and elongation.

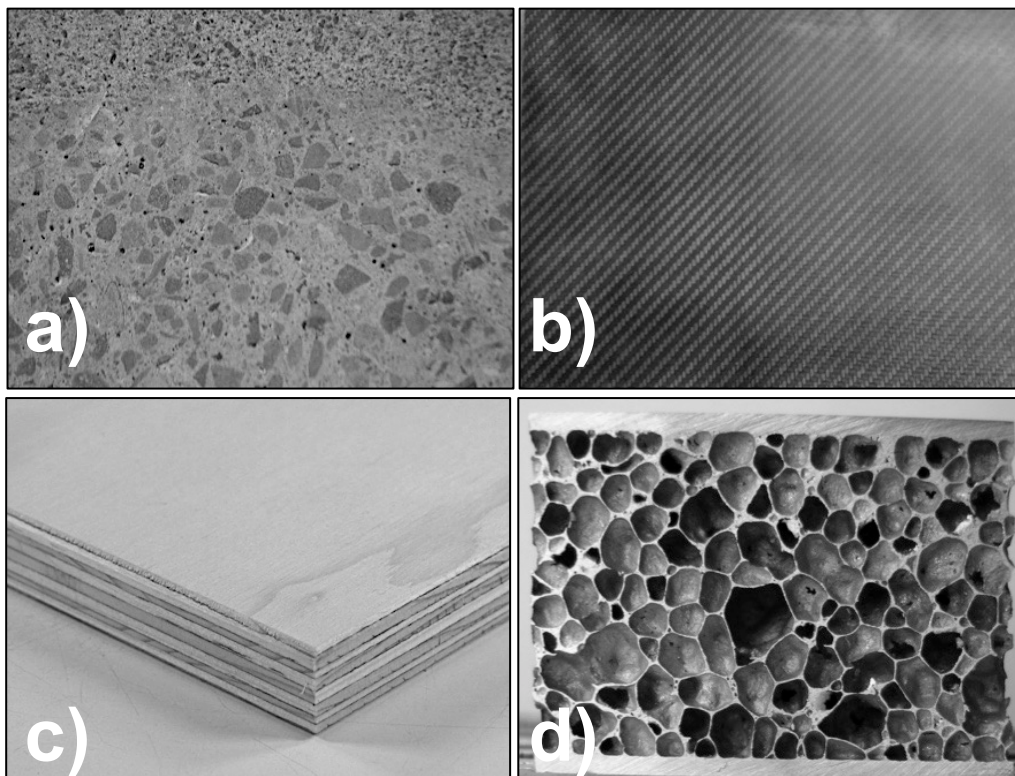


Figure 1. Images of the three different classes of composite materials with fillers consisting of: a) particles; b) fibers (© Shearo / Wikimedia Commons / CC-BY-SA-3.0); c) Laminates (fiber) and d) gas.(© Metalfoam / Wikimedia Commons / CC-BY-SA-3.0)

2.2 Medical X-ray shielding composites for personal protection

The basis for protective radiation shielding is to incorporate materials such as concrete, lead or lead impregnated material in amounts that adequately attenuate ionizing radiation. Today

there exists a wide variety of radiation shields for that purpose. The second-generation personnel protection clothes (gloves and garments) is composed of clear lead shields that consist of a transparent lead-plastic composites impregnated with approximately 30 weight percent of lead [10]. As the thickness of this material increases the X-ray shielding or attenuation increases. However, the physical weight of high protective shields of this type may expose the wearer to ergonomic risks as discussed in the introduction. The clear lead shield composites X-ray protection is proportional to its filler dispersion and distribution. A homogenous distribution and dispersion of the filler ensures that the material at all points attenuate the same amount of x-ray (of the same energy). Thus, no radiation leakage at any material zones exists. Any composite intended for x-ray shielding needs to have highest possible distribution and dispersion of its filler. Filler distribution and dispersion in composite materials is discussed in section 2.3 Mixing: Distribution and Dispersion.

2.3. Mixing: distribution and dispersion

Mixing is a key step in many polymer process. The state of mixing affects material properties, and processability; this will be discussed later in this section. Solid additives are usually available as agglomerates of particles [11]. Break up of agglomerates can be achieved by generating hydrodynamic forces above the individual particles cohesive forces. The hydrodynamic forces for a spherical particle suspended in liquid can at low Reynolds numbers (<1 , slow viscous flow) be described as [12]:

$$F_{hydro} = 6\pi\mu Ur_p \quad (1)$$

Where, μ = is the coefficient of viscosity, U = relative fluid velocity with respect to particle and r_p = particle radius. From equation (1) it is clear that particle size, viscosity of the matrix (polymer) the particle is suspended in and mechanical energy (stress) introduced to the system affect the hydrodynamic force the particles are exposed to. At this stage it is also important to define Reynolds number. Reynolds number account for the importance for inertial and viscous forces and is a number characteristic of the flow of a fluid in a pipe or past an obstruction. Reynolds number can be described as [12]:

$$\text{Reynolds number} = \frac{\text{inertial forces}}{\text{viscous forces}} = \frac{\text{fluid density} \times \text{speed} \times \text{size}}{\text{viscosity}} \quad (2)$$

It is important to mention that the particle shape which is neglected in equation (1) is known to be an important factor affecting hydrodynamic force [12]. Fragmentation of agglomerates can in its simplest form be described as [11]:

$$F_{rag} = \frac{\sigma_{hf}}{\sigma_c} \quad (3)$$

Where σ_{hf} = hydrodynamic force induced into the system (flow) and σ_c = cohesive force of the agglomerates. This fragmentation process (F_{rag}) proceeds through two different mechanisms. Either particles detach from large agglomerate or the agglomerates break into several smaller clusters [11, 13]. The fragmentation process is also indicated to be reversible and can be pictured to proceed according to Figure 2 [12, 14].

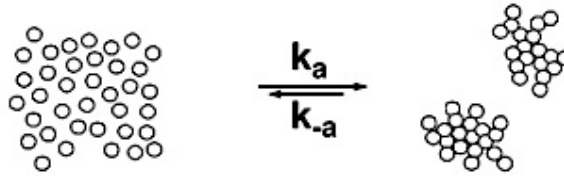


Figure 2. Schematic of reversible fragmentation and agglomeration

Distribution and dispersion can be understood and explained by Figure 3. It has been shown that filler dispersion and distribution influence polymer composites properties, such as electrical conductivity, impact resistance, elasticity, tensile strength etc [15-17]. One of the main goals in the preparation of composites has therefore been directed towards achieving uniform filler dispersion and distribution, see Figure 3. Even though many methods to improve filler dispersion have been explored, it is difficult to compare and evaluate the different dispersion and distribution methods and select the best method [15-17].

Dispersion evaluation techniques proposed and reported has in many cases been based on evaluation of specific material properties specific for the type of material prepared and investigated. Raman mapping of carbon nanotube CNT based nanocomposites is one example that has been reported [18, 19]. However, the problem with many of the specific methods for

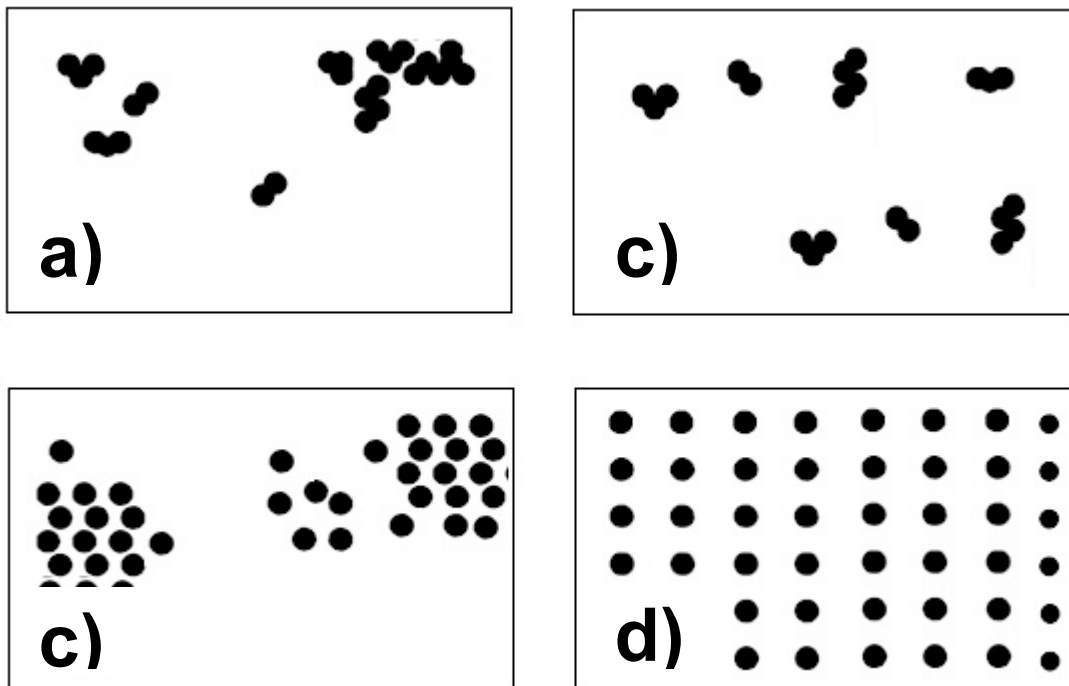


Figure 3. a) Bad dispersion and bad distribution. b) Bad dispersion and good distribution, c) good dispersion, bad distribution d) good dispersion and distribution

evaluation of dispersion and distribution, such as Raman mapping, is that the analysis is unspecific in itself. Many other factors could affect the measured properties that are used to evaluate dispersion and distribution. For instance, in the case of a filled composite with a constant loading, slight difference in filler concentration could lead to orders of magnitude

change in electrical conductivity and viscosity. Hence, additional analysis other than specific material properties should be used. It has been reported that dispersion and distribution assessment generally consist of image analysis in three steps:

- a) Images representing the microstructure of composites are captured by microscopes, such as optical microscope (OM), scanning electron microscope (SEM), or X-ray imaging.
- b) From the photo images the fillers can be identified.
- c) Statistical analysis is made of dispersion and distribution.

Several reported methods utilise image software enhancing the contrast between fillers and the polymer matrix and set an image threshold to separate the fillers from the background [20, 21]. By using large areas of images taken with OM and SEM the statistics of the analysis can be improved and the speed and efficiency of the analysis improved. In this work light microscope coupled with computer imaging technique was used to evaluate dispersion and distribution of filler. A statistical method was used to calculate dispersion index [3]. However, a specific material property was also used to analyse dispersion and distribution, viscosity. Apparent viscosity was measured with capillary rheometer.

2.4 Stabilisation of fillers

Agglomeration as discussed previously is generally a problem when working with powder particles, below 1 μm [22]. In order to avoid agglomeration and increase dispersion and distribution one can use a stabilisation methodology. Some methods used to stabilise fillers are listed below [23] and shown in Figure 4.

- a) Electrostatic stabilisation is often used in aqueous media, or media with a high dielectric constant. This kind of stabilisation is achieved by chemical dispersants that produce strong repulsive electrostatic forces between powder particles.
- b) Steric stabilisation is mostly used in organic media. Organic molecules are adsorbed on the powder surface. The efficacy of the stabilisation is influenced by the affinity between the tail of the molecule and the solvent.
- c) Electrosteric stabilisation. This technique is a combination between steric and electrostatic stabilisation.
- d) Depletion stabilisation.

In this study stearic acid ($\text{C}_{18}\text{H}_{36}\text{O}_2$), was used to coat and adsorb on CuO particles according to the second method, steric stabilisation. In order to evaluate the stabilisation method and the effect of different amounts of stearic acid (SA) contact angle measurements was used.

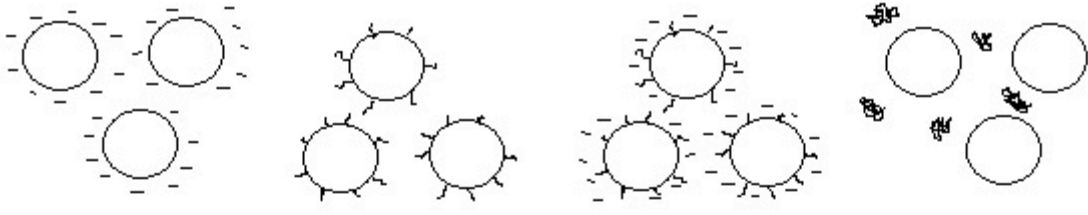


Figure 4. Examples of different methods for powder stabilisation from left to right: electrostatic stabilisation; steric stabilisation; electrosteric stabilisation; depletion stabilisation.

3. Experimental methods and techniques

3.1 Mixing equipment [26, 27]

Mixing equipment was used in order to mix the polymer matrix with the filler material particles. Two different types of equipment has been used melt mixer and extruder.

3.1.1 Melt mixer

This type of mixing equipment is used for laboratory experiments and investigations. The melt mixer is cost-effective, reliable and requires a small amount of material. The melt mixer consists of a mixer backstand with a gear unit and a mixer bowl. In order to prevent damage due to overload there is an electronic safety system. The temperature and torque is selected in the device control, and the material filler and polymer is fed in the mixer bowl where it is melted and mixed at the same time. The melt mixer can be equipped with different blades. Depending on the chosen interchangeable blades to be mounted in the mixer, the available volume and shear forces in the chamber varies. The melt mixers used in this work and setup is shown in Appendix V.

3.1.2. Extruder

Generally extruders are used to simulate process equipment on a laboratory scale. There are two main types of extruders single screw and double screw. Figure 5 shows a schematic of a single screw extruder. In the extrusion process the polymer is fed in solid state into the fed funnel (hopper) and goes out of the extruder in a melt state trough the die. The feed section is the closest to the hopper, here the fed is compacted and transported to the next zone. Sometimes the polymer can be fed as a melt originating from a reactor. In other cases solid materials are extruded and the solid melted downstream the extruder. In the compression zone, the deepness of the channel decreases gradually and the pressure increases. The next zone, the metering section homogenise the material under pressure. Processing parameters and conditions such as torque, melt temperature, melt pressure, are recorded continuously and can be viewed *in-situ*. Extruders as well as melt mixers may have interchangeable screw elements. The extruders used in this work are shown in Appendix V.

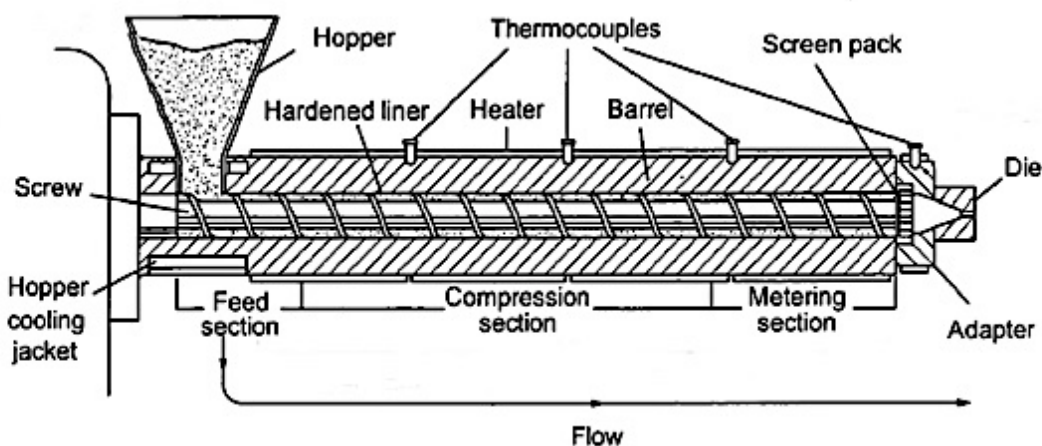


Figure 5. Schematic of a single screw hot melt extruder

3.2. Tensile test [28]

This analysis is done in order to investigate mechanical properties of the produced filaments. The tensile strength of a material is defined as the maximum load that a material can support without fracture divided by the original cross-sectional area of the material. A tensile test involves mounting a specimen in the tensile apparatus and subjecting it to tension. The tensile force is recorded as increase of the gauge length. Increase in gauge length is then converted to strain. Strain is defined as $e = \Delta L/L_0$, where L_0 = is the initial gauge length and ΔL = change in gauge length. Stress is defined as $s=F/A_0$, where F = tensile force and A_0 = initial cross sectional area. When force elongation data is plotted as stress and strain values independent of specimen dimensions are obtained.

3.3 Capillary rheometer [29]

Rheological properties such as viscosity can be measured using a capillary rheometer. Capillary rheometers aim at testing conditions which are representative for processing conditions, especially for high-pressure and high-speed techniques like injection molding; therefore they are key for process optimization. The capillary rheometer consists of a piston-die system that measure viscosity of polymer melts as a function of temperature and rate of deformation. Capillary rheometers are capable of analyzing basic polymers, compounds, various composites with particles or fibers. The basic idea is that a thermoplastic sample under the temperature action transforms to fluid and is forced to flow out of a cylinder through a capillary die. The measured quantity is normally the generated pressure under steady state conditions. A flow curve is the typical output, obtained by interpolation of several experimental data. Viscosity is represented as η and expressed in Pascal seconds (Pa·s) or Newton seconds per square meter (N·s/m²). More information of the type of capillary rheometer analysis used in this work can be found in Appendix III.

3.4 Scanning electron microscopy (SEM) [30]

This microscopy technique is used for the analysis of material microstructure and chemical surface composition. The interesting aspect for this project is to use SEM for analyzing filler shape and size. As well as determine particle size and particle size distribution. The principles for this tool is to use a high energy beam, (called primary electrons), emitted from a filament. The high energy beam is focused on the surface of the sample which is analysed. Different detectors collect secondary and backscattered electrons (SEs and BEs) generated from the high energy beams interaction with the sample surface. The signals produced by the energy beam are transformed to an image. A prerequisite for obtaining an image of the sample is to have a conductive sample or coat the sample with a conductive material, such as gold.

4. Experiments

4.1 Mixing experiments

4.1.1. Melt mixer-Brabender

Melt mixing experiments were primarily performed at CTH and at Swerea IVF. A general mixing procedure consisted of heating up the melt mixer to the desired temperature 100°C, 150°C or 200°C. Then at a low rpm (25 rpm) add the polymer. When the entire polymer had been added and melted the CuO powder was added. The CuO powder was introduced gradually in the mixing chamber. When all the CuO powder had been added the rpm was increased to 60, 180 or 250. And the mixing allowed to continue up to 20 min. For instrument setup see Appendix V.

4.1.2. Extruder

Extrusion experiments were performed at CTH and Swerea IVF. Only CuO-EVA28-25 composite with a loading of 10 vol.% was processed. CuO and EVA28-25 was melt mixed according to the procedure described in previous section at Swerea IVF. Then the material was granulated by hand. A general extrusion procedure consisted of first assembling the dice package (1 nozzle; 1.5 mm) and heating up the extruder zones (CTH: 130°C-140°C-150°C-150°C; Swerea IVF 130°C-140°C-150°C-150°C-150°C). Then insert extruder screw and mount the die package. After this the extruder screw rotation was started (CTH 30 rpm; Swerea IVF approximately 30 rpm) and CuO-EVA28-25 pellets continuously added to the fed funnel. The filaments obtained after exiting the nozzle were allowed to cool in air.

4.2 Image analysis

4.2.1. Liquid dispersion analysis

CuO powder (1, 2, and 3wt.%) was added to a test tube containing liquid (water, ethanol or toluene). The test tube was sonicated for 5 min. A drop of the sonicated dispersions was put on a piece of microscopy glass (OM analysis) or a tip holder fitted with carbon paste (SEM analysis).

4.2.2. Composite image analysis

Melt mixed and extruded CuO-EVA28-25 composites were placed in a metallic beaker fitted with teflon plastic at the bottom. The beaker was heated in an oven at 180°C for approximately 10 minutes. When the CuO-EVA28-25 composite had melted it was taken out from the oven and pressed by hand force between two pieces of teflon plastic. Then samples were viewed on a Leitz DMRX optical microscope and images taken at a magnification of x5, x10, x20 and x50.

Also cross section was analysed with the optical microscope, even though from this analysis conclusions could not be drawn. This may be due to the way the samples were cut; a smooth surface could not be obtained with the technique available.

4.3 Capillary rheometer experiments

Small pieces of the sample material were loaded into the bore of the capillary rheometer. The capillary die length was 10 mm and the diameter 2 mm. The rheometer analysis was generally performed at 150 °C. The pressure steps due to change in shear rates was carefully monitored during operation. Extended time was allowed for the rheometer to find a stable viscosity value.

4.4 Coating of particles

Iso-propanol (30.0 g) and Stearic Acid (0.52 g) was added in that order to a beaker. The mixture was first agitated on a stirrer plate for 5 minutes. Then moved to a sonificater and sonificated 5 minutes. Then CuO (10.0 g) was added to the beaker. After CuO addition the mixture was agitated 5 minutes on a stirrer plate and sonificated 5 minutes. The beaker was then put on the stirrer plate and at stirred until all Iso-propanol (>24h) had evaporated and only dry stearic acid coated CuO powder remained.

4.5 Tensile testing

Tensile testing was performed at Swerea IVF. The general procedure was to cut up 10 cm long filaments pieces (obtained at the capillary measurement), measure the diameter at 3, 6 and 9 cm and then load the filaments onto the apparatus load cell. The strain gauge was set to 25 mm (25 mm of filament between the grips) and rate set to 250 mm/min.

5. Results and Discussion

5.1 Materials

In this work ethyl vinyl acetate grade EVA28-25 polymer was used as matrix or binder for the CuO filler. EVA28-25 is a random copolymer synthesized from ethylene monomer and vinyl acetate co-monomer. EVA copolymers represent the largest volume segment of the ethylene copolymer market. In this study ethyl vinyl acetate with a vinyl acetate content of 27-29 wt.% was used. Characteristics of the EVA28-25 polymer are listed in Table 1. Two CuO products with different particle size distributions were used: Copper (II) oxide provided by Fluka-Analytical and Copper (II) oxide powder supplied by Sigma-Aldrich.

The CuO filler particles were analysed with SEM see Figure 6. As apparent from Figure 6 the particles from Fluka Analytical, shown in Figure 6b) was larger than the ones supplied by Sigma-Aldrich. The SEM images shown in Figure 6 were used to construct histograms in order to more precisely determine the CuO filler particle size distributions. Figure 7a and 7b show the constructed histograms. For the Sigma-Analytical material it is seen that the mean is 0.9 μm and the particle size range 0.2-2.2 μm . The histogram for the Fluka-Analytical material shows that mean is 3.3 μm and the particle size range 1.0-31.0 μm . Table 2 list the mean, standard deviation, median, mode and range of the particle size for both materials.

Table 1. Properties of EVA28-25 supplied by manufacturer ARKEMA

| Characteristics | Value | Unit | Test Method |
|-----------------------------|----------|-------------------|------------------------|
| Vinyl Acetate content | 27-29 | Weight% | FTIR (Internal Method) |
| Melt Index (190C/2.16 kg) | 22-29 | g/10min | ISO 1133 / ASTM D1238 |
| Density (23°C) | 0.95 | g/cm ³ | ISO 1183 |
| Melting point | 71 | °C | ISO 11357-3 |
| Vicat softening point (10N) | <40 | °C | ISO 306 / ASTM D1525 |
| Ring and Ball temperature | 120 | °C | ASTM E28 / NF EN 1238 |
| Elongatin at break | 800-1000 | % | ISO 527 / ASTM D638 |
| Tensile strength at break | 14 | MPa | ISO 527 / ASTM D639 |
| Hardness Shore A | 75 | - | ISO 868 / ASTM D2240 |

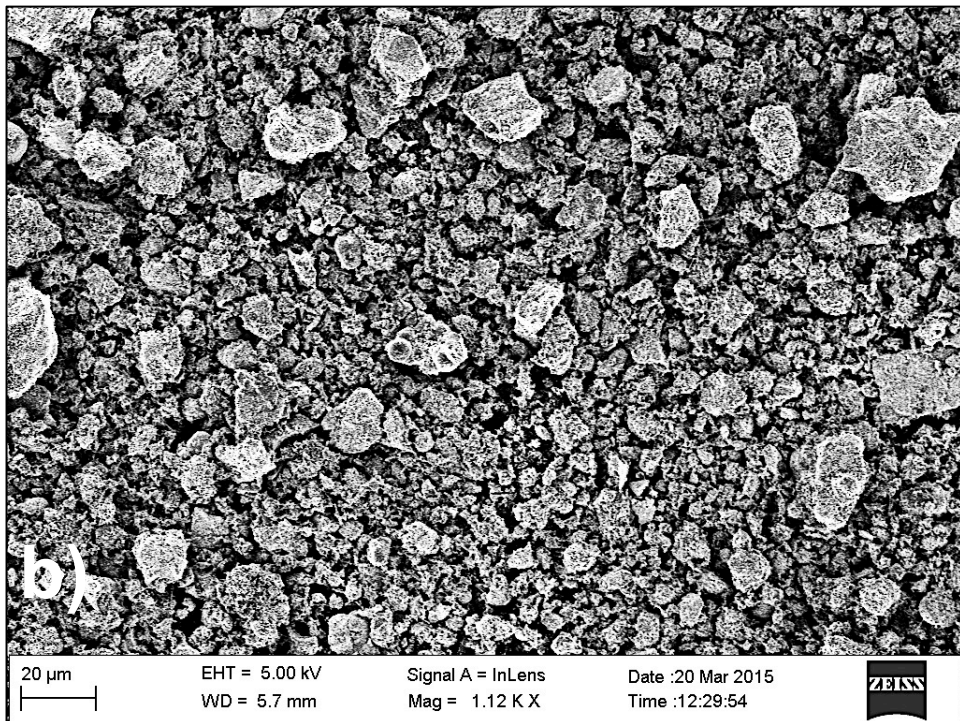
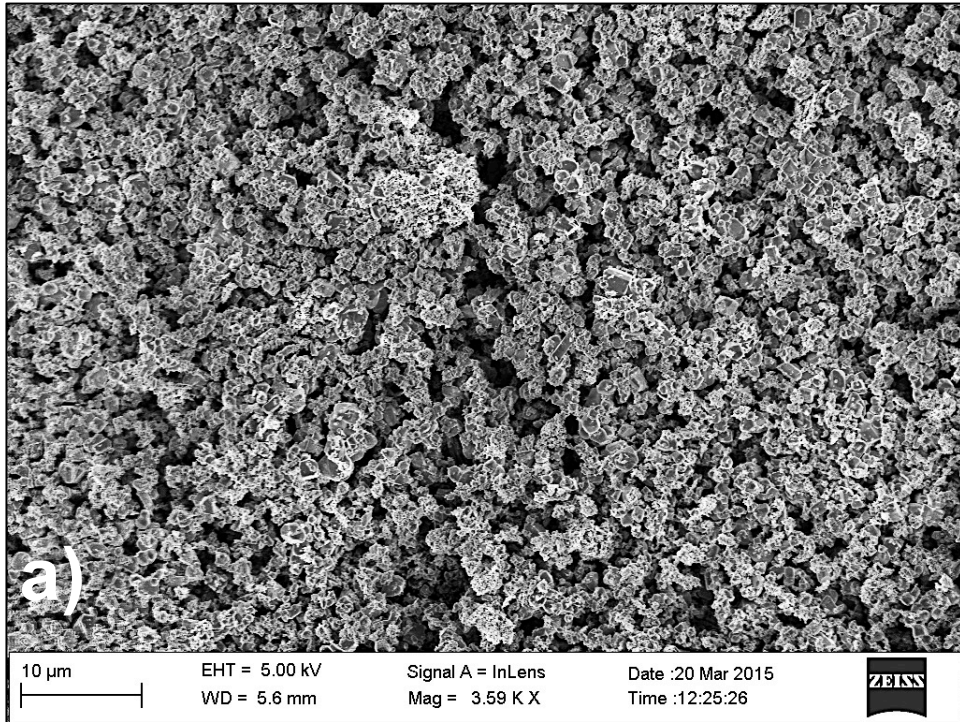


Figure 6. SEM images of CuO powder supplied from a) Sigma-Aldrich and b) Fluka-Analytical.

Table 2. CuO products characteristics as determined by SEM analysis

| Product | Mean (μm) | STD (μm) | Median (μm) | Mode (μm) | Range (μm) |
|------------------|------------------------|-----------------------|--------------------------|------------------------|-------------------------|
| Fluka-Analytical | 3.3 | 4.4 | 1.0 | 1.0-1.5 | 1.0-31.0 |
| Sigma-Aldrich | 0.9 | 3.2 | 0.5 | 0.2-0.4 | 0.0-2.2 |

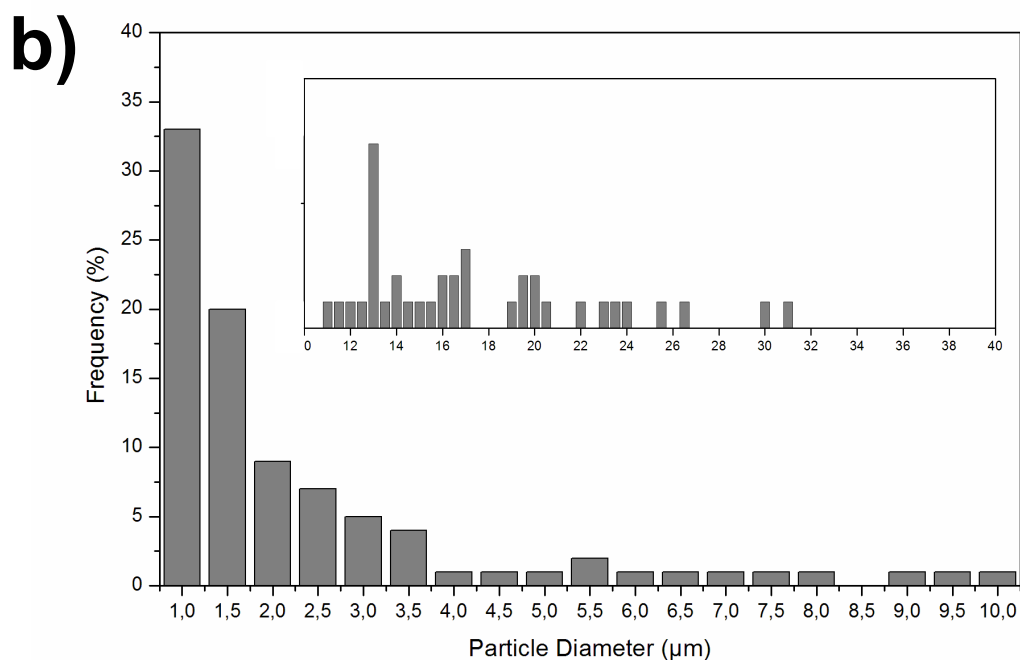
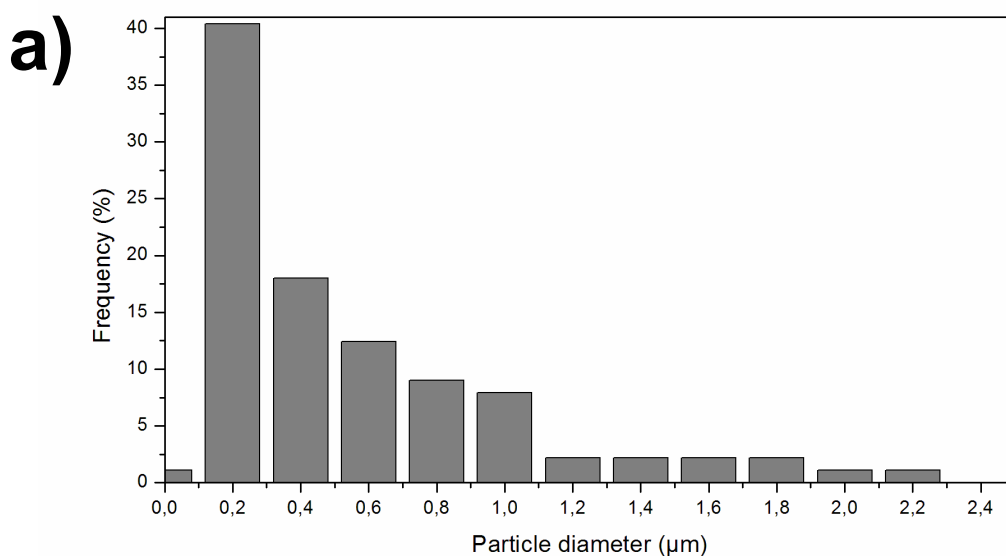


Figure 7. Particle size histograms of a) CuO powder provided by Sigma-Aldrich and b) by Fluka Analytical.

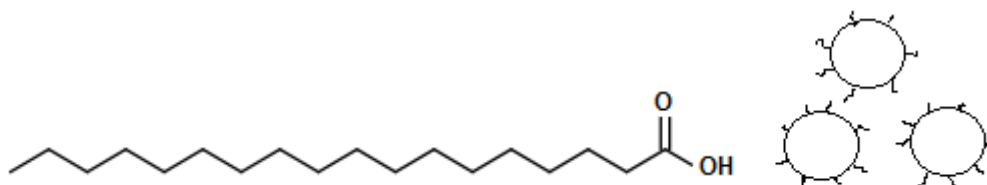


Figure 8. Molecular structure of Stearic Acid (SA) and Schematic of spherical particles of powder coated with SA.

5.2 Coating filler

In order to achieve high dispersion and distribution in the matrix used in this study the filler particles needed to be stabilised. In this study steric stabilisation was used to minimise agglomeration of the CuO filler particles. Stearic acid (SA) has been used before as an additive in Powder Injection Moulding (PIM) processing [22]. The stearic acid molecule consists of 18 linear carbon atoms and a carboxylate acid end group, see Figure 8. Figure 9 show the effect of various amounts of SA on CuO powders. Figure 9 shows that when increasing the amount of SA from 1wt.% to 5wt.% an increase in the contact angle is obtained from initially 85 to 130 degrees. The contact angle is generally adopted to evaluate the effect of surface modifier on inorganic fillers. High contact angle means that the distilled water does not wet the surface, which is beneficial for the compatibility of the CuO powder with the mostly nonpolar polymer matrix (EVA28-25). When increasing the amount of SA further above 5 wt.% the contact angle decrease. Uncoated CuO powder is hydrophilic, while the coated powder is more hydrophobic and therefore disperses better in a hydrophobic polymer matrix. Microscopy analysis was performed on uncoated and coated CuO powder in order to validate that SA stabilised and dispersed the CuO powder. Figure 10 shows binary microscopy dispersion images of uncoated CuO powder (Figure. 10a) and 5 wt.% SA coated CuO (Figure 10b). The coating procedure reduces agglomeration behaviour of the CuO powder.

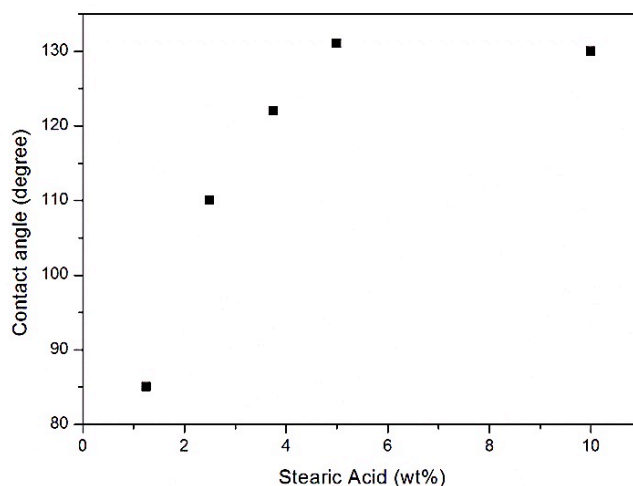


Figure 9. Measured contact angle plotted as contact angle vs. stearic acid (wt.%).

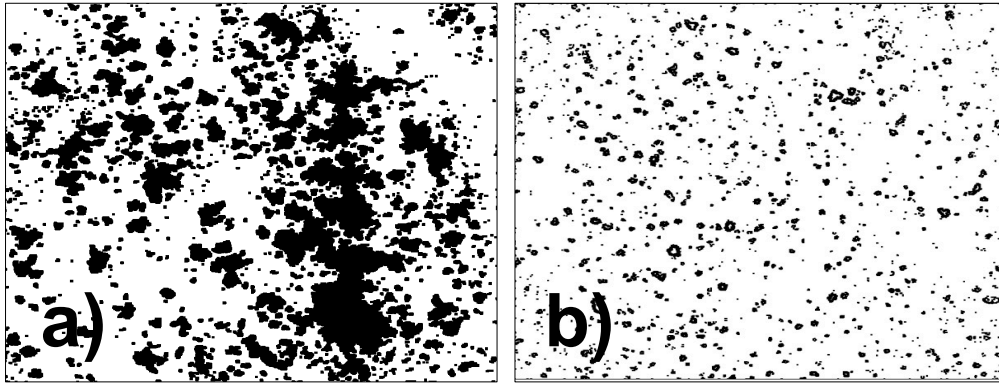


Figure 10. OM binary microscopy images of 1 wt.% powder dispersed in toluene. Image: a) shows CuO powder and b) shows CuO powder coated with 5wt.% stearic acid

5.3 CuO-EVA28-25 composites

A number of parameters were investigated such as mixing time, temperature, rpm, particle loading, particle size, particle coating and process equipment setup. Light microscope (OM) and capillary rheometer was used to analyse the mixing (filler dispersion and distribution) as a function of the preparation parameters. Figure 11 shows the results from the initial analysis. Figure 11a shows CuO and EVA28-25 mixed for 5 minutes. As can be seen, the polymer and CuO are not properly mixed. Figure 11b shows CuO and EVA28-25 mixed 10 minutes. After 10 minutes of mixing in the melt mixer a macroscopically homogenous composite is obtained. After many experiments it was found that the proper mixing of both materials happens after 10 minutes in the Brabender melt mixer. Table 4 highlight a problem during the experimental analytical work. Table 4 list conditions and amounts as well as determined n and K values from capillary rheometer experiments. As can be seen in the Table measurements on the same material taken at different days gave different results (1 and 2). However, analysing materials prepared at different times the same day gave very similar results (2 and 3). Some artefacts were observed at low shear rates, as expected. In order to get reliable data all comparing measurements were therefore made at the same time. Therefore the same composite material may have different viscosity values in the Tables.

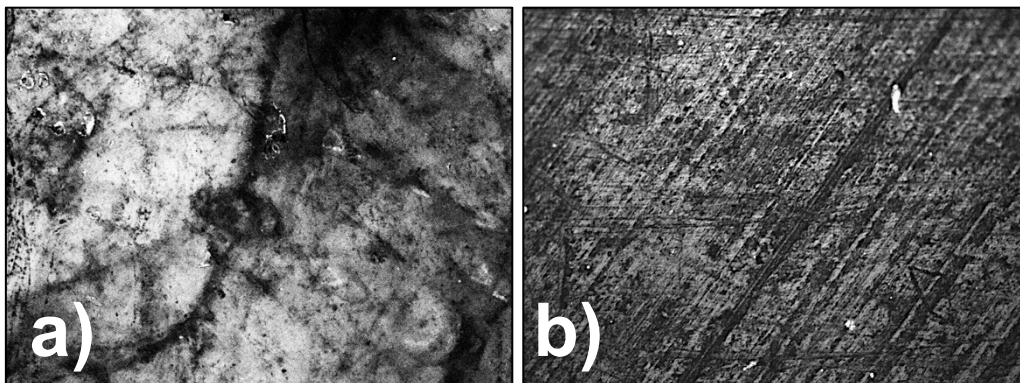


Figure 11. Image a) shows melt mixed filler and polymer before macroscopically homogenous composites were obtained (mag. x20) and Image b) shows macroscopically homogenous melt mixed filler (1wt.%) and polymer.

Table 4. Conditions, amounts and results for initial melt mixed CuO-EVA28-25 composite material analysed with capillary rheometer

| Experiment | Date | Amounts (g) | | Conditions | | Constants ($\eta=K\dot{\gamma}^{n-1}$) | | | |
|------------|--------------------|-------------|------|--------------------------|------------|--|-------|-------|-------|
| | | CuO | EVA | Rpm (min ⁻¹) | Temp. (°C) | Time (min) | n | K | R (%) |
| | March | | | | | | | | |
| 1 | 5 th | 23.4 | 35.0 | 60 | 150 | 20 | 0.175 | 45113 | 95.23 |
| 2 | 19 th a | 23.4 | 35.0 | 60 | 150 | 20 | 0.603 | 2838 | 99.93 |
| 3 | 19 th b | 23.4 | 35.0 | 60 | 150 | 20 | 0.620 | 2867 | 99.54 |

5.4 Mixing time

Conditions and results from dispersion analysis are listed in Table 5. Selected microscopy images can be found in Appendix IV. Experiments at 5, 10 and 20 minutes were made at two different volume loadings of filler 1.0% (1.5g CuO and 22.5g EVA polymer) and 0.2% (0.4g CuO and 22.5g EVA polymer). As can be seen in Table 5 at 1.0 vol.% loading best mixing is received after 20 minutes. While the experiments at 0.2 vol.% show that best mixing is achieved after 10 minutes. It was more difficult to analyse the images at 1.0 vol.%. No further image analysis at 1.0 vol.% was therefore prepared and performed. The result indicates that a lower filler loading gives more reliable and interpretable results. The results are therefore interpreted as best mixing (highest dispersion and distribution) is achieved between 10 to 20 minutes.

5.5 Temperature

Conditions and results from dispersion analysis and capillary rheometer analysis are listed in Table 5. Selected microscopy images can be found in Appendix IV. Attending to the temperature, experiments with low filler loading (0.2 vol.%) were performed and samples were taken after 20 min of mixing at 100°C, 150°C and 200°C. From the image analysis and the calculated image dispersion index best results are obtained at 150°C. Melt mixing at a medium temperature results in a better distribution. The lowest K value and highest n value was obtained at 150°C. The K value at 100°C is also low but when the temperature is increased to 200°C a higher K value is obtained. The n value does not display a linear temperature behavior trend.

5.6 Rotation rate (RPM)

Conditions and results from dispersion analysis and capillary rheometer analysis are listed in Table 5. Selected microscopy images can be found in Appendix IV. When studying how the velocity of the flow affects the mixing of CuO-EVA28-25 composites, experiments with low filler loading (0.2 vol.%) was prepared for image analysis at 60, 180 and 250 rpm in the melt

mixer. The dispersion index indicates that at a lower velocity of the fluid the mixing is better. This may be seen as contradictory with equation (1) in section 2.3 Mixing: Distribution and Dispersion. Equation (1) states that higher fluid velocity or shear increases the hydrodynamic forces and increase de-agglomeration. However, it is not clear whether the difference in speed of moving particles in fluid and surrounding fluid is higher at 250 rpm than at 60 rpm. Furthermore, as Figure 2 shows the agglomeration and de-agglomeration is a reversible process. The dispersion index analysis correlates with the results from the capillary rheometer analysis. Where one can see that the lowest value for K and highest n value is obtained at 60 rpm compared to measurement taken for materials prepared at 180 and 250 rpm.

5.7 Particle loading

Conditions and results from dispersion analysis and capillary rheometer analysis are listed in Table 6. In order to validate the viscosity analysis as well as investigate the behavior of the composite at higher filler loadings, experiments with pure polymer composites and mixtures with CuO with loadings ranging from 5 to 20 vol.% was prepared and analyzed. The results in Table 6, show that increasing the amount of filler loading also increases the value of K. The n value reduces from 5-20 volume% filler.

Table 5. Conditions, amounts and results from time, temperature and RPM experiments in melt mixer for CuO-EVA28-25 composites

| Experiment | Amounts (g) | | Conditions | | | Constants ($\eta=K\dot{\gamma}^{n-1}$) | | | Dispersion D 0.1-0.2 |
|-------------------------|-------------|------|-----------------------------|------------|---------------|--|------|-------|-------------------------|
| | CuO | EVA | Rpm (min ⁻¹) | Temp. (°C) | Time (min) | n | K | R (%) | |
| Time experiments | | | | | | | | | |
| 1 | 1.5 | 22.5 | 60 | 150 | 5 | - | - | - | 0.3 |
| 2 | 1.5 | 22.5 | 60 | 150 | 10 | - | - | - | 0.6 |
| 3 | 1.5 | 22.5 | 60 | 150 | 20 | - | - | - | 1.8 |
| 4 | 0.4 | 30.0 | 60 | 150 | 5 | - | - | - | 0.5 |
| 5 | 0.4 | 30.0 | 60 | 150 | 10 | - | - | - | 3.4 |
| 6 | 0.4 | 30.0 | 60 | 150 | 20 | - | - | - | 2.8 |
| Temperature experiments | | | | | | | | | |
| 7 | 23.4 | 35.0 | 60 | 100 | 20 | 0.665 | 3050 | 99.27 | - |
| 8 | 23.4 | 35.0 | 60 | 150 | 20 | 0.696 | 2772 | 92.63 | - |
| 9 | 23.4 | 35.0 | 60 | 200 | 20 | 0.641 | 3341 | 99.30 | - |
| 10 | 0.4 | 30.0 | 60 | 100 | 20 | - | - | - | 2.1 |
| 11 | 0.4 | 30.0 | 60 | 150 | 20 | - | - | - | 2.8 |
| 12 | 0.4 | 30.0 | 60 | 200 | 20 | - | - | - | 0.6 |
| RPM experiments | | | | | | | | | |
| 13 | 23.4 | 35.0 | 60 | 150 | 20 | 0.699 | 2703 | 95.33 | - |
| 14 | 23.4 | 35.0 | 180 | 150 | 20 | 0.648 | 3163 | 98.73 | - |
| 15 | 23.4 | 35.0 | 250 | 150 | 20 | 0.619 | 3824 | 95.33 | - |
| 16 | 0.4 | 30.0 | 60 | 150 | 20 | - | - | - | 2.8 |
| 17 | 0.4 | 30.0 | 180 | 150 | 20 | - | - | - | 0.7 |
| 18 | 0.4 | 30.0 | 250 | 150 | 20 | - | - | - | 0.2 |

5.8 Particle size

Results from the study of the particle size influence are shown in Table 6. Better results are obtained with the Fluka-Analytical product (mean 3.3 μm ; range 1.0-31.0 μm). The reason for that could be that the packing becomes better with a larger size distribution. According to equation (1) the larger the particle radius the higher the resulting hydrodynamic force should be. And therefore should also a better mixing be received as indicated by the n and K values.

5.9 Particle coating

Results from the particle coating experiments are shown in Table 6. From the Table it can be seen that as long as the amount of SA increase the lower the K and higher n value become. That indicates that complete stearic stabilization give best mixing. This correlate well with the image analysis used for validating the stabilization protocol shown in Figure 10.

5.10 Extrusion experiments

Conditions and results from dispersion analysis and capillary rheometer analysis are listed in Table 7. Samples first melt mixed were extruded in two different extruder instrument setups. All experiments were carried out with composites with 10 vol.% of filler. The viscosity analysis show that, as expected a better mixing is received after extruding the samples in comparison only melt mixed composites. Between the two extruder setups the one at CTH gives better results than the Swerea IVF extruder. The reason is because of the geometry of

Table 6. Conditions, amounts and results from filler loading, particle size and SA coating experiments in melt mixer for CuO-EVA28-25 composites

| Experiment | Parameter | Amounts (g) | | Conditions | | | Constants ($\eta=K\dot{\gamma}^{n-1}$) | | |
|--------------------------------------|-----------|-------------|------|---------------------------|------------------------------|------------|--|-------|-------|
| | | CuO | EVA | Rpm (min^{-1}) | Temp. ($^{\circ}\text{C}$) | Time (min) | n | K | R (%) |
| Volume (%) filler | | | | | | | | | |
| 1 | 0% | 0.0 | 45.0 | 60 | 150 | 20 | 0.612 | 2693 | 99.56 |
| 2 | 5% | 15.0 | 45.0 | 60 | 150 | 20 | 0.641 | 2832 | 99.56 |
| 3 | 10% | 23.4 | 35.0 | 60 | 150 | 20 | 0.560 | 6046 | 99.52 |
| 4 | 20% | 35.0 | 26.2 | 60 | 150 | 20 | 0.507 | 9332 | 99.87 |
| Particle size (mean, μm) | | | | | | | | | |
| 5 | 0.9 | 23.4 | 35.0 | 60 | 150 | 20 | 0.325 | 18840 | 97.07 |
| 6 | 3.3 | 23.4 | 35.0 | 60 | 150 | 20 | 0.540 | 5623 | 99.69 |
| CuO Coated with stearic acid (%) | | | | | | | | | |
| 7 | 0 | 23.4 | 35.0 | 60 | 150 | 20 | 0.324 | 18836 | 98.04 |
| 8 | 50 | 23.4 | 35.0 | 60 | 150 | 20 | 0.479 | 7566 | 99.87 |
| 9 | 100 | 23.4 | 35.0 | 60 | 150 | 20 | 0.559 | 4757 | 99.55 |

Table 7. Conditions, amounts and results from extrusion experiments in compounder for CuO-EVA28-25 composites

| Experiment | Amounts (g) | | Conditions | | Constants ($\eta=K\dot{\gamma}^{n-1}$) | | | |
|---------------|-------------|-------|------------------------------|------------------------------|--|-------|------|-------|
| | CuO | EVA | Rpm (min^{-1}) | Temp. ($^{\circ}\text{C}$) | Time (min) | n | K | R (%) |
| Melt mixing | 23.4 | 35.0 | 60 | 150 | 20 | 0.691 | 5591 | 99.85 |
| Extrusion CTH | 180.0 | 230.0 | 30 | 130-140-150-150 | 20 | 0.693 | 4929 | 99.87 |
| Extrusion IVF | 180.0 | 230.0 | 30 | 130-140-(150) ₃ | 20 | 0.697 | 4335 | 99.32 |

the extruder rods, look at Appendix V.

5.11 Tensile testing

From the capillary viscometer measurements filaments were collected. Selected filaments were tested for their tensile strength. The data is collected and listed in Table 8. In this Table results from pure EVA-28-25 (sample 1) is also shown as a reference. As can be seen filler particle size influences the materials tensile strength. Comparing samples 3 and 7 higher values of peak and breaks stress are obtained with materials prepared with the CuO powder with a mean of 0.9 μm . This fact means that the filaments melt mixed with smaller particles are stronger than the ones prepared with the larger filler particles 3.3 μm . However, the results is not conclusive since the number of measurements are few and the difference between the samples are small. The results also contradict known facts. This tensile test curves has a maximum strength. The maximum strength in this curve correspond to the break stress and not peak stress. There is a variation between the different tensile strength runs, which can explain the results.

Previously in this work it has been demonstrated that the coating of the powder with stearic acid results in a better mixing (distribution and dispersion) of the filler in the polymer matrix. From the tensile test measurements it is seen when comparing samples 3, 4 and 5 as much as the presence of SA increase in the sample higher peak and break stress values are obtained. However, small differences were found between 0% and 50% of SA coating (samples 3 and 4). The third parameter analyzed with tensile testing was the filler loading. Samples 1, 2, 3 and 6 were prepared with loadings ranging from 0-20 wt.%. When increasing the loading lower values of break and peak stress are obtained. This means that, in general, the amount of filler deteriorate composite properties, as expected.

However in the case of the maximum loading, 20 vol.% no deterioration of tensile strength properties can be observed compared to 10 vol.%. In fact a small increase in the tensile strength value is obtained. This fact is probably due to statistical reasons and related to number of measurements performed as can be understood from the standard deviation. The result does not mean that the properties are better at higher loadings. Microscopy analysis was carried out on the several filaments obtained from the capillary rheometer; the images are shown in Figure 12. Comparing a) and b), with and without filler, the texture of the filament has changed. Between samples c) and d) one can see the effect of the SA coating, but from

Table 8. Composition parameters effect on tensile tests of CuO-EVA28-25 composite filaments

| Sample | Filler | | | Tensile strength results | | |
|--------|------------|------------------|--------------------------------------|--------------------------|-----------------|--------------------|
| | Volume (%) | Stearic acid (%) | Particle size (mean, μm) | Peak stress (MPa) | Elongation (mm) | Break stress (MPa) |
| 1 | 0 | 0 | - | 7.270 | 6.756 | 7.125 |
| 2 | 5 | 0 | 0.9 | 6.231 | 6.756 | 5.668 |
| 3 | 10 | 0 | 0.9 | 6.001 | 6.752 | 5.440 |
| 4 | 10 | 50 | 0.9 | 6.591 | 6.836 | 5.443 |
| 5 | 10 | 100 | 0.9 | 6.869 | 6.744 | 6.168 |
| 6 | 20 | 0 | 0.9 | 6.139 | 6.752 | 5.670 |
| 7 | 10 | 0 | 3.3 | 5.707 | 6.816 | 5.399 |

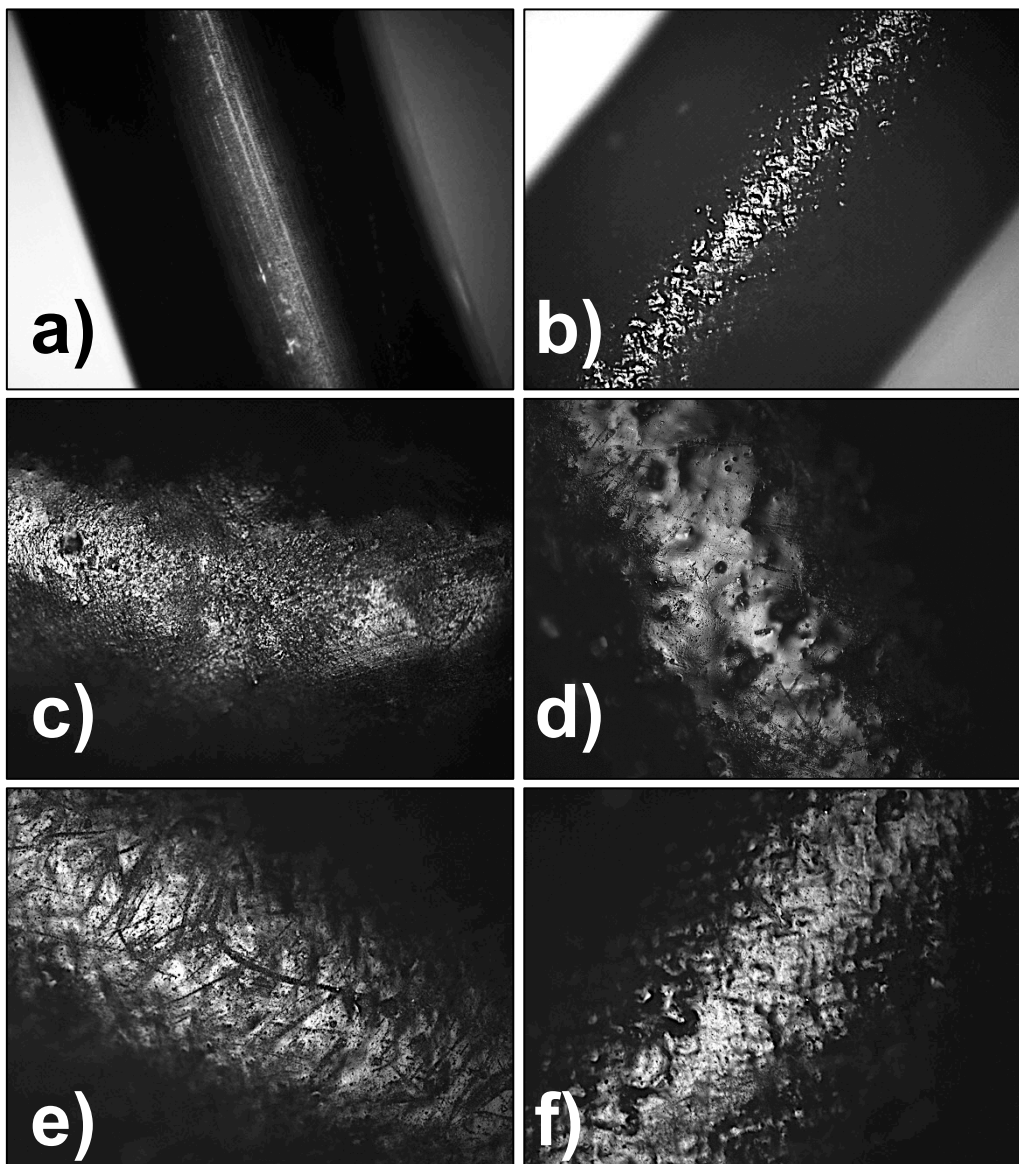


Figure 12. OM images of CuO-EVA28-25 composite filaments: a) EVA28-25 mag x5; b) CuO-EVA28-25, 10 vol.%, particle size 0.9 μm , mag x5; c) CuO-EVA28-25, vol.% 10%, 100% SA coated CuO, particle size 0.9 μm , mag x20; d) CuO-EVA28-25, 10 vol.%, particle size 0.9 μm , mag x20; e) CuO-EVA28-25, 10 vol.%, particle size 3.3 μm , mag x20; f) CuO-EVA28-25, 20 vol.%, particle size 0.9 μm , mag x20.

This analysis no clear results can be drawn. Samples d) and e) have the same filler loading loadbut different particle size. The filaments for the bigger filler material show a more coarse texture. When comparing image c) and f), it is seen that the higher the loading, the more rude the texture becomes.

6. Conclusions

From the present investigation the following conclusions could be drawn:

Analysis

Light microscope together with appropriate imaging software could be used to evaluate degree of mixing for low filler loaded composites.

Capillary rheometer could be used to evaluate degree of mixing for high filler loaded composites.

A strong correlation was seen between the mixing parameters of low loaded filler composites analysed with light microscope and high filler loaded composites analysed with capillary rheometer.

Mixing Parameters

Improved mixing was achieved after 10 minutes of low speed mixing at a medium temperature. The comparing melt mixing with a Brabender melt mixer and an extruder, showed that extrusion gave better mixing results. Particle coalescence had minor significance during the latter material processing. Larger particle size distributions gave better mixing results (distribution and dispersion).

Stabilisation methodology

The dispersion and distribution of CuO in EVA polymer strongly depended on the dispersability of the as-received CuO material. The surface properties of CuO were improved by adding suitable surface modifier (stearic acid). The obtained results, from the optical images, rheology measurements and from the tensile test show that the particle coating or powder stabilisation resulted in a better dispersion and distribution and composite materials with better mechanical properties.

7. Suggestions for future work

Higher particle contents would be interesting to study further in order to gain more understanding of influence on the dispersion and distribution for material intended for a commercial product.

X-ray studies should be done in order to gain information about the protection properties of the performed materials, since the methods applied to evaluate the dispersion and distribution of the filler only provide information of the surface of the materials and materials mechanical properties.

It would be interesting to try more dispersants.

8. References

- [1] A. Kyle Jones and Louis K. Wagner, *Medical Physics* (2013) 40, 063902.
- [2] M. Saiyad, N. M. Devashrayee, R. K. Mevada, *Polymer Composites* (2014) 1264-1266.
- [3] *Composites Science and Technology* “Method of quantitative analysis of filler dispersion in composite systems with spherical inclusions” Volume 71, Issue 13 (2011) 1543–1549.
- [4] Y. Y. Huang, E. M. Terentjev, *Int. J Mater Form* (2008), 1, 63–74.
- [5] Y. Y. Huang, S. V. Ahir, and E. M. Terentjev, *Physical Review B* (2006), 73, 125422-1-125422-9.
- [6]. R.N. Rethon, Ed., *Particulate-Filled Polymers*, Rapra Technology, Shawbury (2003).
- [7]. A.K. Kulshreshtha and C. Vasile Ed., *Handbook of Polymer, Blends and Composites*, Rapra Technology, Shawbury 1(2002).
- [8] *Fundamentals of Fibre Reinforced Composite Materials*, Escrito por A.R. Bunsell, J Renard
- [9] http://web.mit.edu/course/3/3.064/www/slides/composites_overview.pdf
- [10] *Radiation protection , in medical radiography*, Elsevier, M.A. Statkiewicz Sherer, P. J. Visconti, E. R. Ritenour,
- [11] *Predicting Distributive and Dispersive Mixing in Polymer Extrusion*. Natalia Domingues, António Gaspar-Cunha, José António Covas. *AIP Conference Proceedings* 908, 1531 (2007); doi: 10.1063/1.2741026.
- [12] *Mechanics of fluids and transport processes*, Volume 1 1983 Low Reynolds number hydrodynamics with special applications to particulate media.
- [13] N. Domingues, M. Camesasca, M. Kaufman, I. Manas- Zloczower, A. Gaspar-Cunha and J. A. Covas, *Modelling Agglomerate Dispersion in Single Screw Extruders*, Proceeding of ANTEC 2006 Conference, 2006.
- [14] Sven Pegel, Petra Po'tschke, Gudrun Petzold, Ingo Alig, Sergej M. Dudkin, Dirk Lellinger, *Polymer* 49 (2008) 974-984.
- [15] Grady BP. *Macromol Rapid Commun* 2010; 31 (3): 247-57.
- [16] Supova M, Martynkova GS, Barabaszova K. *Sci Adv Mater* 2011; (3): 1-25.
- [17] Moniruzzaman M, Winey Kl. *Macromolecules* 2006; 39 (16):5194-205.
- [18] Linton D, Driva P, Sumpter B, Ivanov I, Geohegan D, Feigerle C, et al. *Soft Matter* 2010; 6 (12): 2801-14.
- [19] Gershon Al, Cole DP, Kota AK, Bruck HA. *J Mater Sci* 2010;45(23): 6353-64
- [20] Pegel S, Potschke P, Vilmow T, Stoyan D, Heinrich G. *Polymer* 2009; 50 (9): 2123-32.
- [21] Sul IH, Young JR, Song YS. *Carbon* 2011;49 (4): 1473-8.
- [22] E. Johansson , *Surface Interactions in Powder Injection Moulding*. 2002; 20-24.
- [23] R.J Pugh, “Dispersion and Stability of Powders in Liquids”, *Surface and Colloid Chemistry in Advanced Ceramics Processing*, R. J. Pugh and L. Bergström (eds.), Marcel Dekker, New York, 1994, pp 127-192.
- [24] R.J Pugh, “Dispersion and Stability of Powders in Liquids”, *Surface and Colloid Chemistry in Advanced Ceramics Processing*, R. J. Pugh and L. Bergström (eds.), Marcel Dekker, New York, 1994, pp 71-125.
- [25] *Dispersions: Characterization, Testing, and Measurement* (Escrito por Erik Kissa 141).
- [26] *Polymer processing: modelling and simulation* by Osswald, Tim A; Hernández-Ortiz, Juan P 2006.
- [27] *Polymer Composites and Polymer Testing*. by Deepak Aggarwal; Hongkui Mao; Lee Menghai, 2012.
- [28] http://www.asminternational.org/documents/10192/3465262/05105G_Chapter_1.pdf/e13396e8-a327-490a-a414-9bd1d2bc2bb8
- [29] Macosko C.W. “*Rheology – Principles, Measurements, and Applications*”, Wiley-VCH (1994).

[30] Joseph I. Goldstein et al., Scanning Electron Microscopy and X-Ray Microanalysis, Ed Plenum 2nd edition 1992.

Appendix I: Quantitative Analysis of Filler Dispersion

Method from: Composites Science and Technology 71 (2011) 1543–1549. Mathematical deduction and explanation.

The probability of a deviation from average should be chosen from the linear region of the probability function $p(a)$ (approx. $0.8-1.2\mu$) and should be kept constant for all the analyzed, images (i.e. $\mu \pm k\mu$ ($0 < k < 1$)).

For any value of k (coefficient) the dispersion parameter (D_k) can be defined:

$$D_k = \int_{\mu(1+k)}^{\mu(1+k)} f(a) da \quad (1)$$

Average particle area is defined according to method as:

$$\mu = \sum_{i=1}^N a_i / N \quad (2)$$

Where a = area of filler particle and N = number of particles. The probability density function is defined as:

$$f(a) = \frac{1}{\sigma\sqrt{2\pi}} \exp\left(-\frac{1}{2}\left(\frac{a-\mu}{\sigma}\right)^2\right) \quad (3)$$

Where σ for μ is defined as:

$$\sigma = \sqrt{\frac{\sum_i (a_i - \mu)^2}{N - 1}} \quad (4)$$

If $z = (a - \mu)/\sigma$ then $dz = da/\sigma$ and D_k the dispersion parameter can be described:

$$D_k = \int_{-k\frac{\mu}{\sigma}}^{+k\frac{\mu}{\sigma}} \frac{1}{\sqrt{2\pi}} \exp\left(-\frac{z^2}{2}\right) dz = \frac{1}{\sqrt{\pi}} \int_{-k\frac{\mu}{\sigma}}^{+k\frac{\mu}{\sigma}} \exp\left(\left(-\frac{z}{\sqrt{2}}\right)^2\right) d\left(-\frac{z}{\sqrt{2}}\right) \quad (5)$$

For the integration of normal distribution the erf function can be used:

$$\text{erf}(x) \equiv \frac{2}{\sqrt{\pi}} \int_0^x \exp(-x^2) dx \quad (6)$$

where $x = +k\frac{\mu}{\sigma}$ and $-k\frac{\mu}{\sigma}$ then the D_k with the erf function become:

$$D_k = \frac{1}{2} \left(\text{erf}\left(\frac{k}{\sqrt{2}}\left(\frac{\mu}{\sigma}\right)\right) - \text{erf}\left(-\frac{k}{\sqrt{2}}\left(\frac{\mu}{\sigma}\right)\right) \right) \quad (7)$$

Equation (7) can be simplified to:

$$D_k = \text{erf}\left(\frac{k}{\sqrt{2}}\left(\frac{\mu}{\sigma}\right)\right) \quad (8)$$

If expressing D_k in the Maclaurin series the expression become:

$$D_k = \frac{2}{\sqrt{\pi}} \sum_{n=0}^{\infty} \frac{(-1)^n \left(\frac{k}{\sqrt{2}} \left(\frac{\mu}{\sigma} \right) \right)^{2n+1}}{n! (2n + 1)} \quad (9)$$

If $\frac{\mu}{\sigma} \leq 2.5$, D_k with precision can be defined as:

$$D_k = \left(\frac{2 x k}{\sqrt{2\pi}} x \left(\frac{\mu}{\sigma} \right) \right) \quad (10)$$

If then k is chosen between as it lies in the linear $p(a)$ region and $k=0.1$ then $D_k=D_{0.1}$ and is defined as:

$$D_{0.1} = \left(\frac{0.2}{\sqrt{2\pi}} x \left(\frac{\mu}{\sigma} \right) \right) \quad (11)$$

Equation (11) has been used in this work to determine the dispersion parameter, k values has been chosen ranging from 0.1-0.2.

Appendix II: Image Analysis Method Validation

Applying Appendix I to light microscope images of dispersions.

$$D_{100}0.1-0.2 = 5.6$$

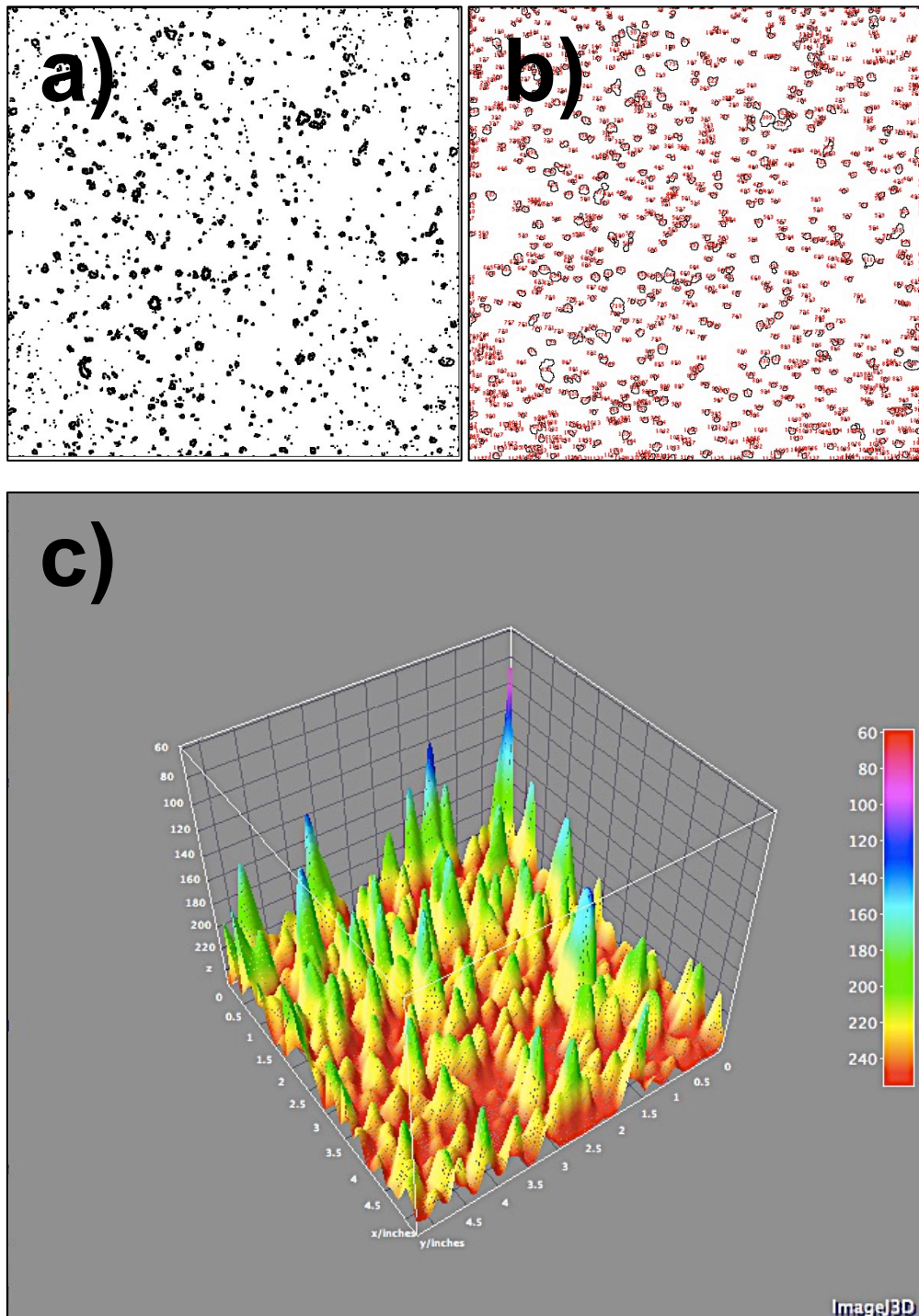


Figure Ap_II 1. a) Binary image of 1 wt.% CuO coated with 5wt.% Stearic Acid dispersed in toluene. b) outline of targeted particles for dispersion and distribution analysis and c) 3D graph of binary image.

$$D_{100}0.1-0.2 = 1.3$$

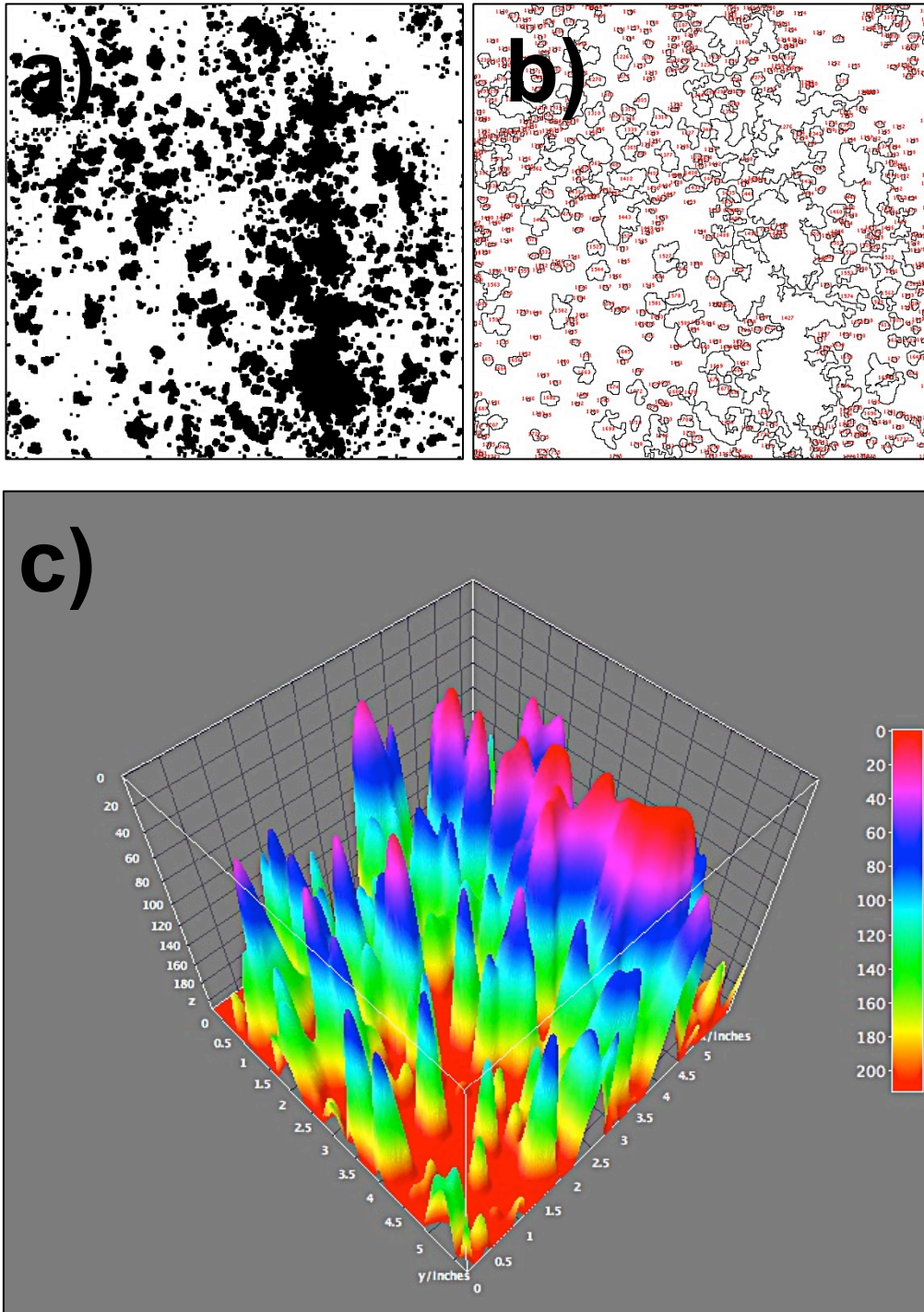


Figure Ap_II 2. a) Binary image of 1 wt.% CuO dispersed 1wt.% in toluene. b) outline of targeted particles for dispersion and distribution analysis and c) 3D graph of binary image.

Appendix III: Capillary Rheometry Analysis and Experimental Determination of Apparent n and K values

Melt Rheology and its Applications in the Plastics Industry ISBN: 978-94-007-6394-4

Viscosity is the rheological property often used to characterize molten plastics. Viscosity measurements provides information about molecular structure and gives valuable information on melt processing parameters. Like all rheological properties the viscosity (and normal stress differences) of a polymer depend on several factors:

i. Flow Conditions

Temperature; Shear rate; Pressure.

ii. Material Composition and Molecular Structure

Molecular weight distribution; Chemical nature of polymer; Presence of long chain branches; Nature and concentration of additives and fillers.

For linear polymers the viscosity curve (on a log–log plot) has a region of essentially constant viscosity as well as a power law region.

The power law region can be described:

$$\sigma = k\gamma^n \quad (1)$$

In terms of viscosity this become:

$$\eta = k(\dot{\gamma})^{n-1} \quad (2)$$

It has been shown that the viscosity and subsequently the n and k values can be correlated with the presence of agglomerates [4,5]. Thus by measuring viscosity, plotting the values on a log-log scale, n and k can be determined. If the flow conditions and material composition is kept constant and only the mixing changed. The n and k values can be used to estimate the distribution and dispersion of the filler.

Appendix IV: Image Analysis Selected Images

Mixing time, temperature and revolutions per minute

Selected Images from mixing time, temperature and revolutions per minute experiments. The theory in Appendix I: Quantitative Analysis of Filler Dispersion, is applied and the procedure described in Appendix II: Image Analysis Validation to calculated dispersion index of OM images on low filler CuO-EVA28-25 composites.

Mixing time (minutes)

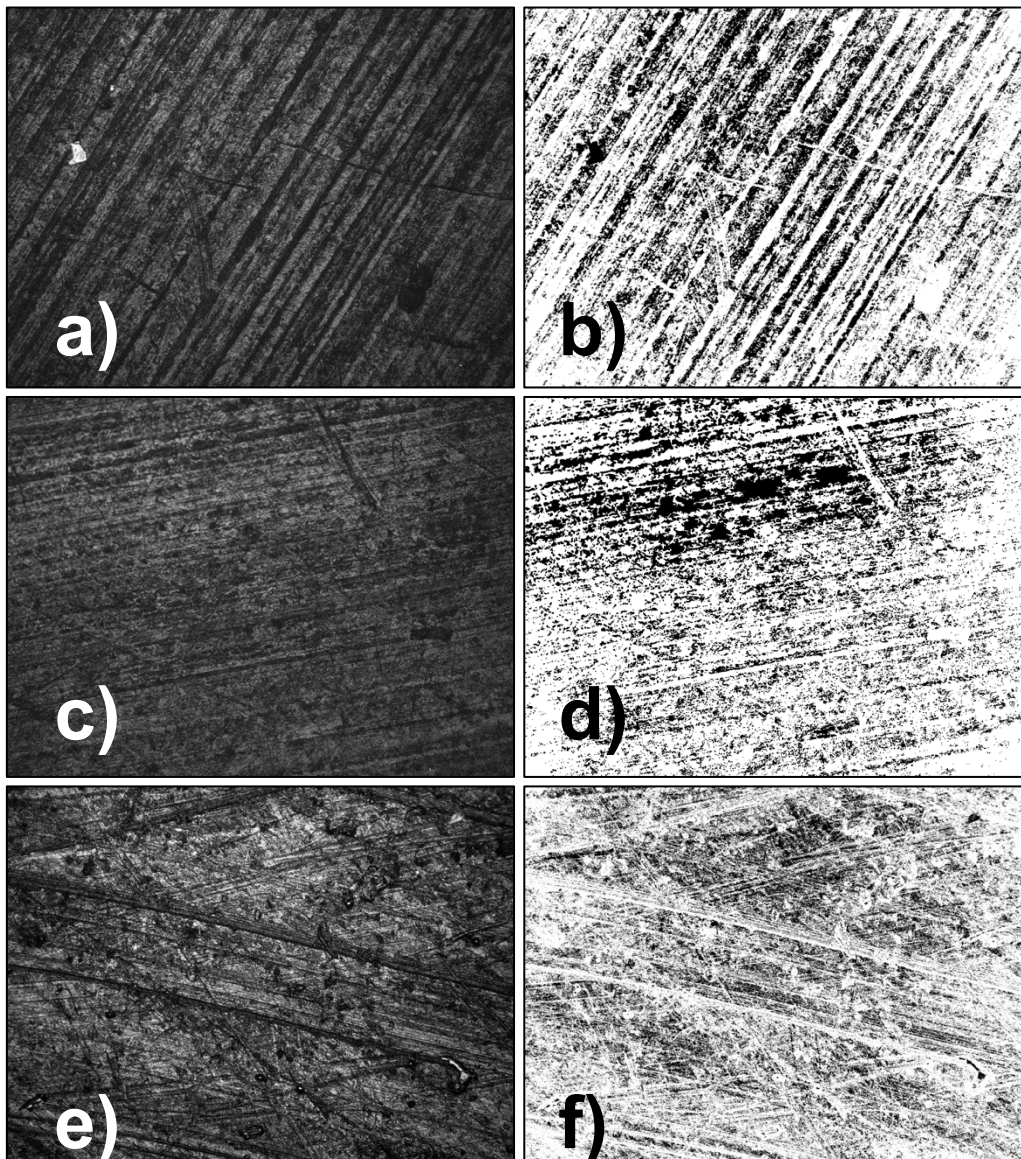


Figure Ap_IV 1. Images taken with SEM with 20x of magnification after: a and b) 5 minutes of mixing; c and d) 10 minutes; and f) 20 minutes of mixing. Image a, c and e show OM microscopy images and b, d and f binary images.

Temperature (°C)

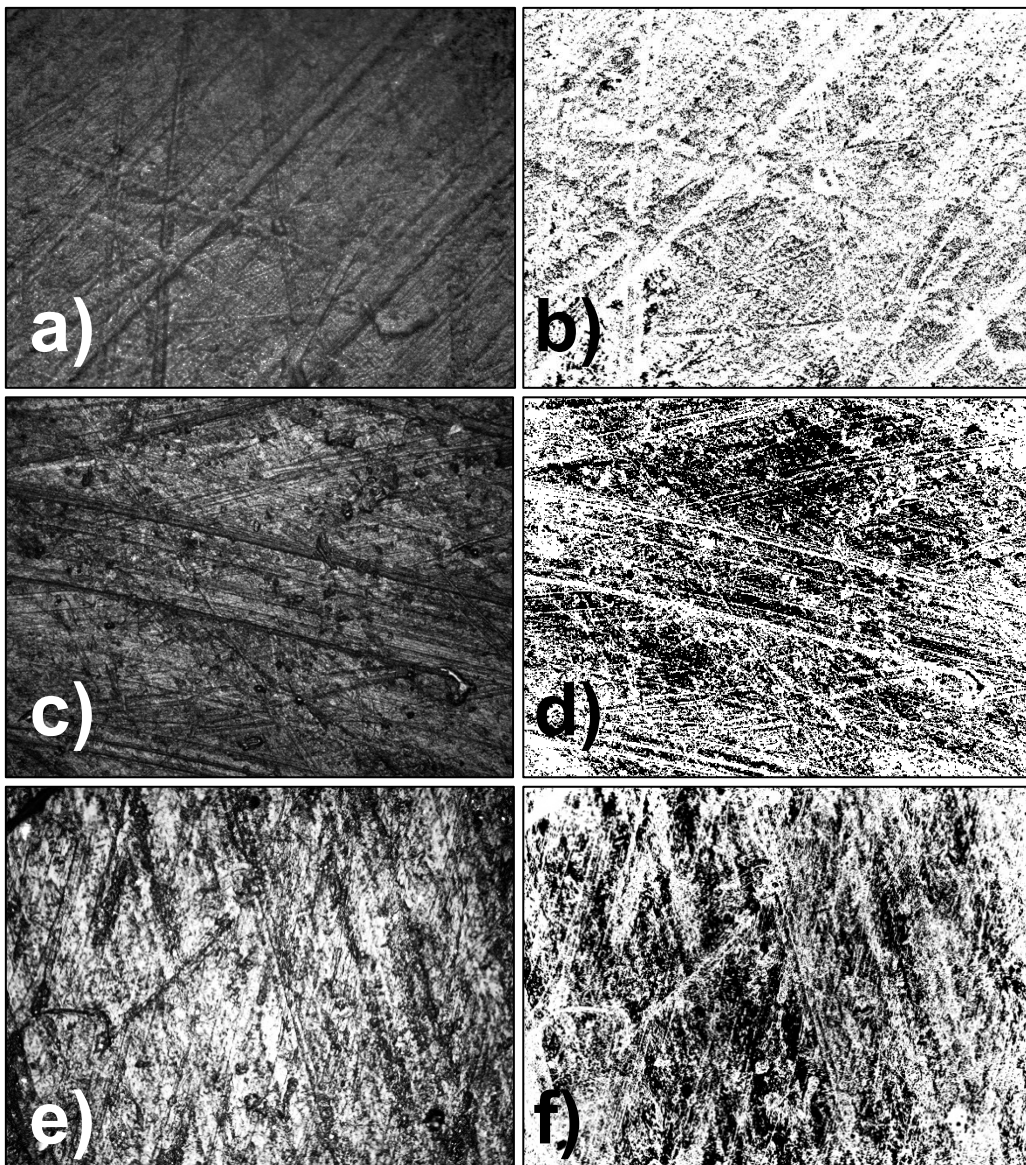


Figure Ap_IV 2. Images taken with SEM with 20x of magnification melt mixed at: a and b) 100°C; c and d) 150°C; e and f) 200°C. Image a, c and e show OM microscopy images and b, d and f binary images.

Revolutions per minute (RPM)

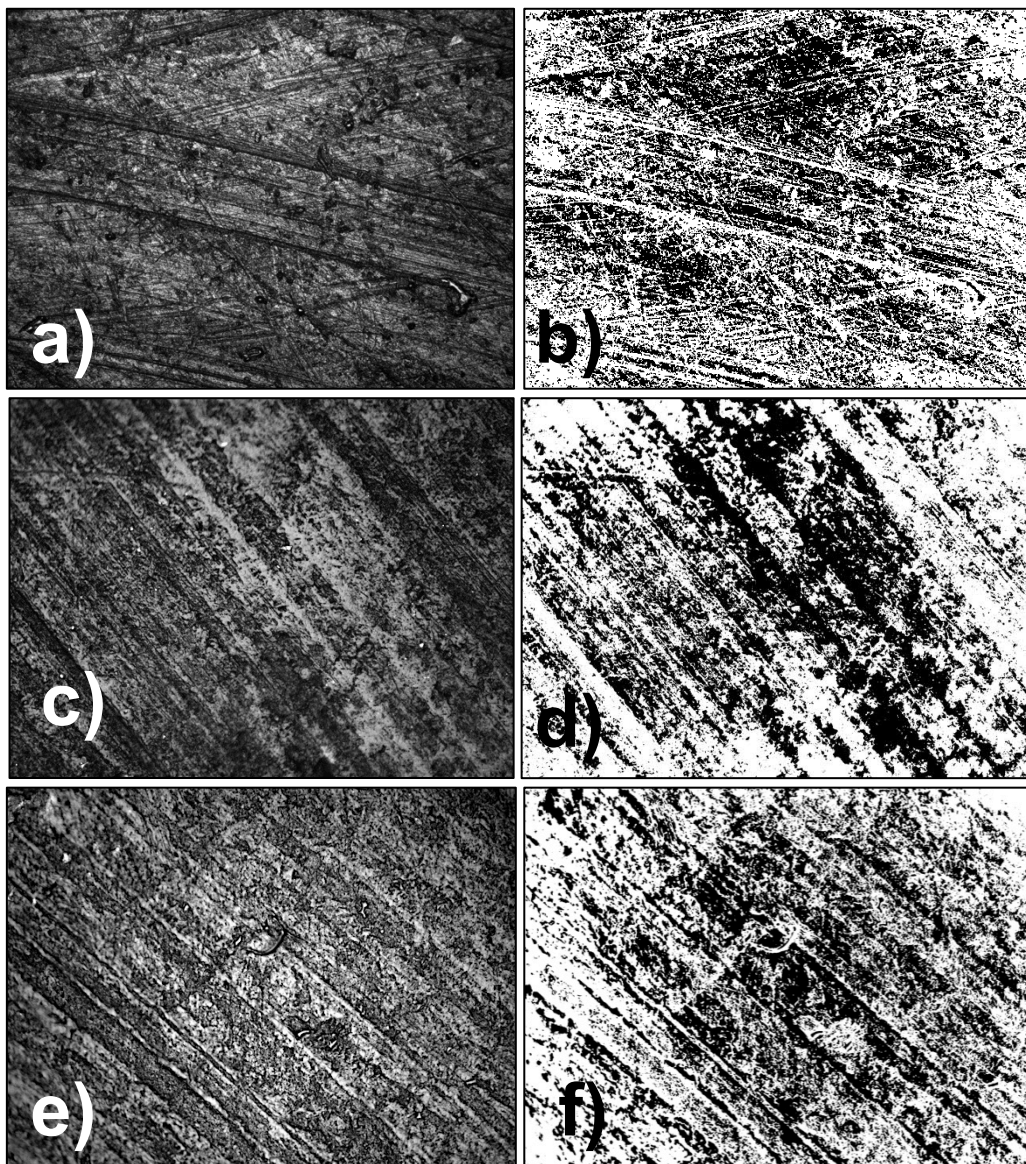


Figure Ap_IV 3. Images taken with SEM with 20x of magnification melt mixed at: a and b) 60 rpm; c and d) 180 rpm; e and f) 250 rpm. Image a, c and e show OM microscopy images and b, d and f binary images.

Appendix V: Manufacturing Equipment

Chalmers University of Technology Mechanical and Manufacturing and Technology
Brabender Meltmixer

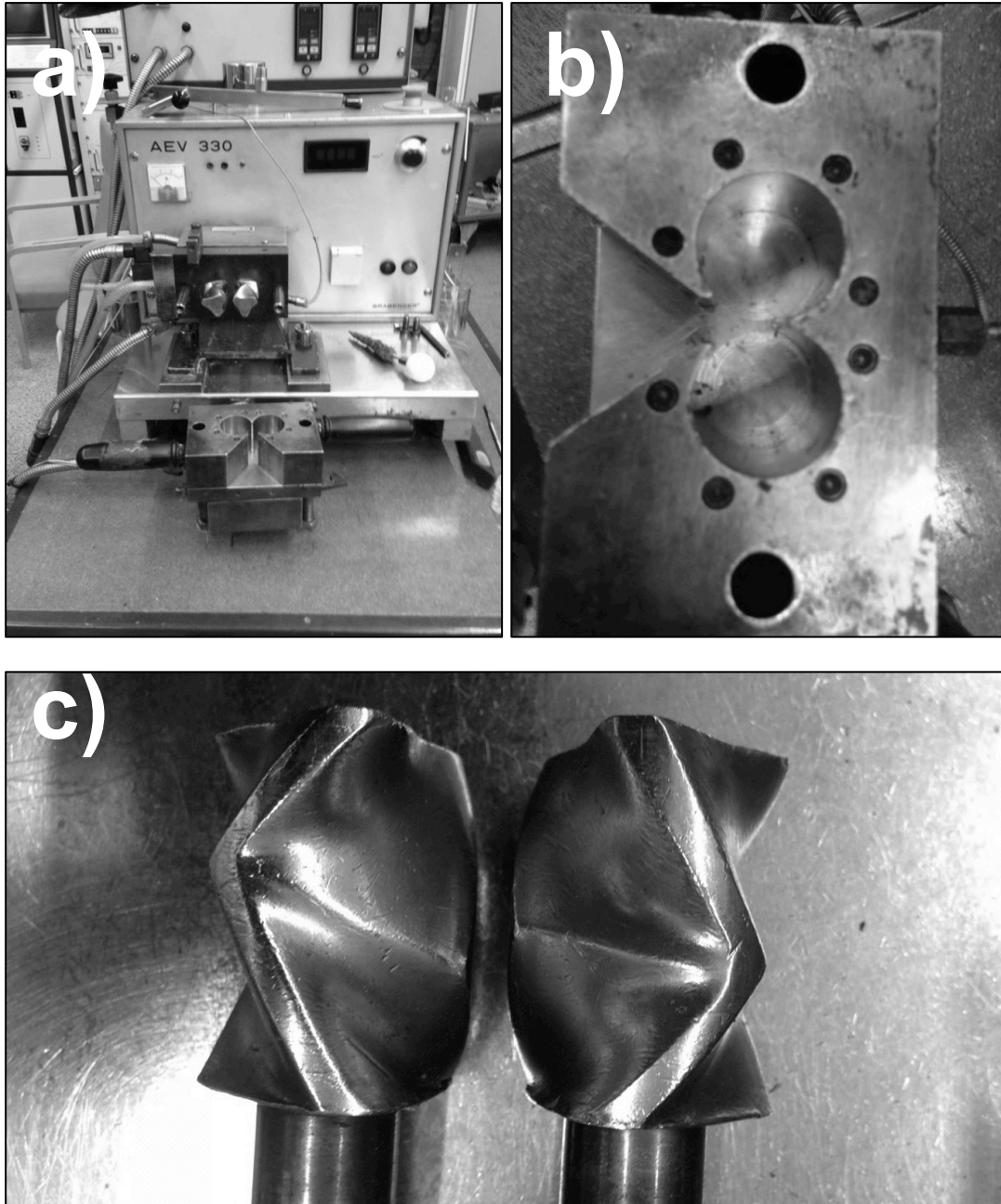


Figure Ap_V 1. Images a) and b) show the Brabender mixer used for the compounding studies. Image c) show the roller blade setup was used. Roller blades are used for materials that require a strong shear force to form a homogenous melt.

Chalmers University of Technology Mechanical and Manufacturing and Technology **Single Screw Extruder**

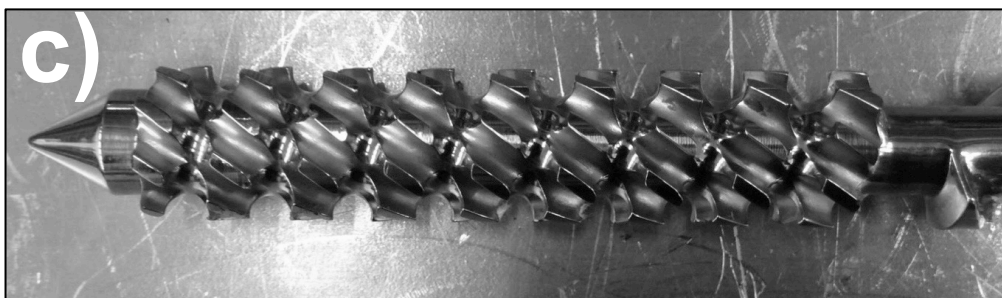
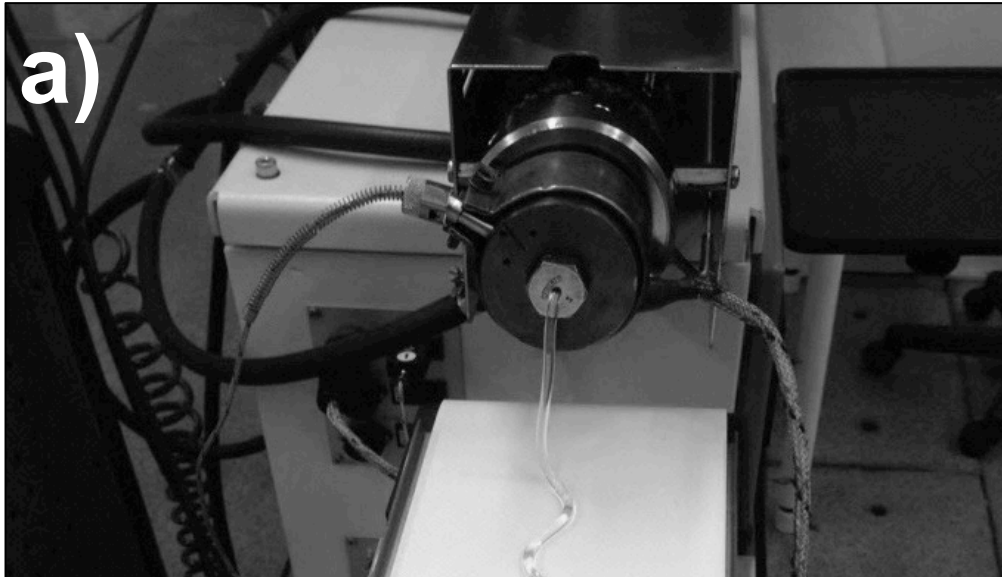


Figure Ap_V 2. Image a) show the single screw extruder used for extruding experiments. Image b) and c) show the extruder rod used. Image b) show that the extruder rod has three zones in addition to the feed zone (not shown in the picture) compression, metering zone and homogenization zone also shown in image c).

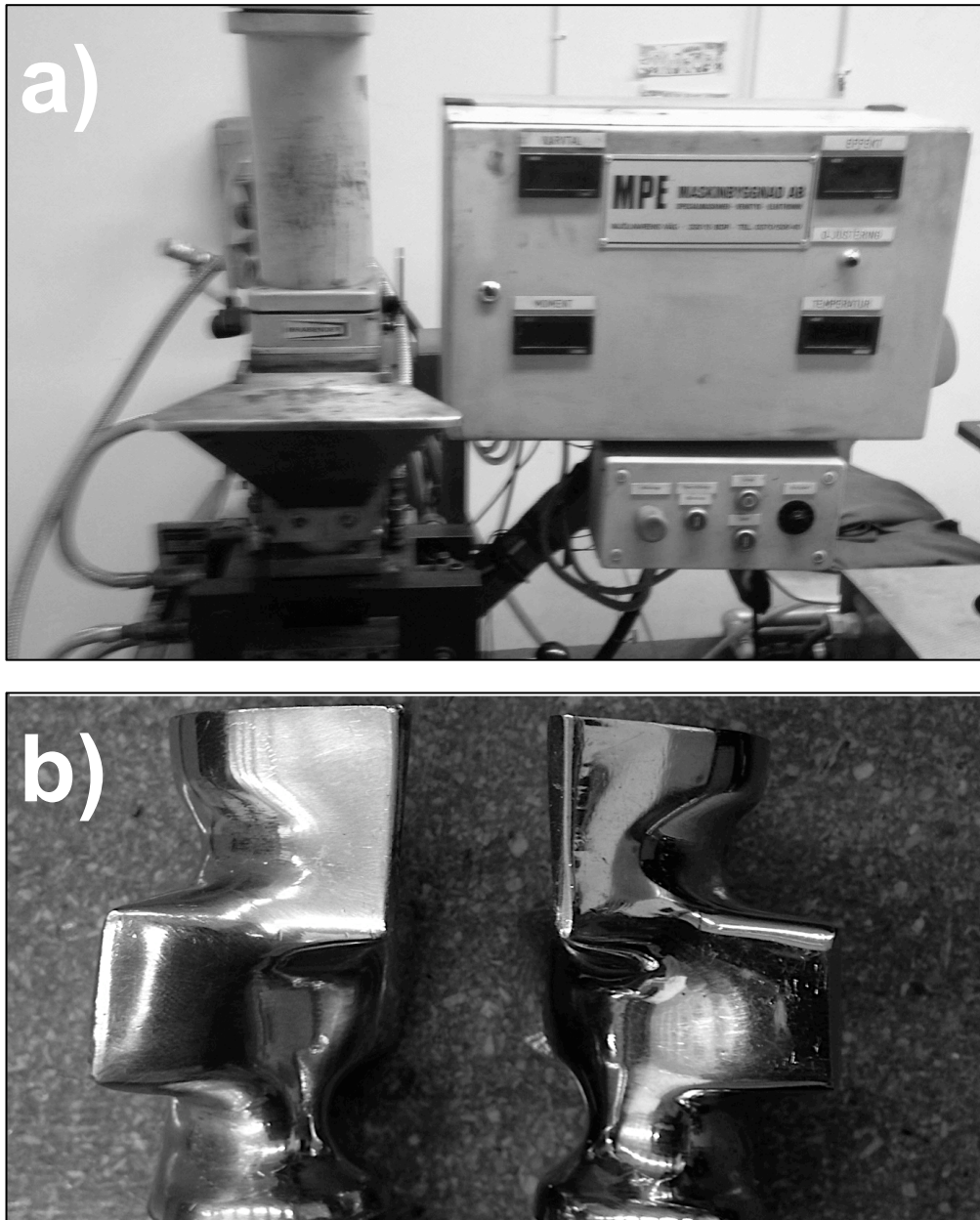


Figure Ap_V 3. Images a) show the Brabender mixer used for the mixer studies. Image b) show the cam blade setup used. CAM Blades impose a combination of milling, mixing, and medium sheare forces against the sample, alternating and compacting.

Swerea IVF Mölndal Textile and Polymers Department **Single Screw Extruder**

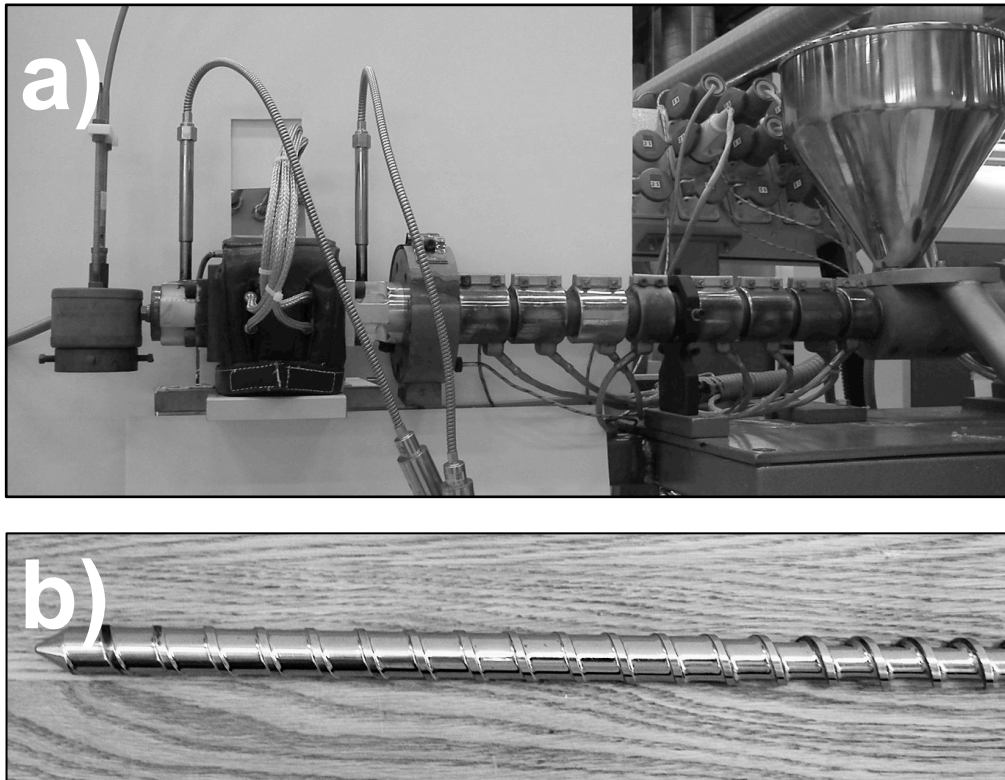


Figure Ap_V 4. Image a) show the single screw extruder used for extruding experiments at SWEREA IVF. Image b) show the extruder rod used. Image b) show that the extruder rod has two zones in addition to the feed zone; a compression and metering zone.